J. Fluid Mech. (1968), *vol.* 32, *part* 4, *pp.* 625–655
Printed in Great Britain

The axisymmetric convective regime for a rigidly bounded rotating annulus

By MICHAEL E. McINTYRE†

Department of Applied Mathematics and Theoretical Physics,
University of Cambridge

(Received 17 June 1967 and in revised form 15 November 1967)

The axisymmetric flow of liquid in a rigidly bounded annular container of height H, rotating with angular velocity Ω and subjected to a temperature difference ΔT between its vertical cylindrical perfectly conducting side walls, whose distance apart is L, is analysed in the boundary-layer approximation for small Ekman number $\nu/2\Omega L^2$, with $g\alpha\Delta T H\nu/4\Omega^2 L^2\kappa \sim 1$. The heat transfer across the annulus is then convection-dominated, as is characteristic of the experimentally observed 'upper symmetric regime'. The Prandtl number ν/κ is assumed large, and H is restricted to be less than about $2L$. The side wall boundary-layer equations are the same as in (non-rotating) convection in a rectangular cavity. The horizontal boundary layers are Ekman layers and the four boundary layers, together with certain spatial *averages* in the interior, are determined independently of the interior flow details. The determination of the latter comprises a 'secondary' problem in which viscosity and heat conduction are important throughout the interior; the meridional streamlines are not necessarily parallel to the isotherms. The secondary problem is discussed qualitatively but not solved. The theory agrees fairly well with an available numerical experiment in the upper symmetric regime, for $\nu/\kappa \doteq 7$, after finite-Ekman-number effects such as finite boundary-layer thickness are allowed for heuristically.

1. Introduction

When a temperature difference ΔT is imposed between the perfectly conducting inner and outer vertical cylindrical boundaries of a rotating liquid-filled annulus (see figure 1 below) several different types of flow can result, as is well known (Hide 1958; Fultz *et al.* 1959; Fowlis & Hide 1965; Lambert & Snyder 1966). For certain regions in the space of governing parameters, the flow can be steady and axisymmetric; in other regions there appear non-axisymmetric regular or irregular wave-like motions. There has been a great deal of experimental and theoretical work on these flows, largely connected with the fact that they have been found to be relevant to the problem of understanding the general circulations of planetary atmospheres such as the Earth's.

† Now at Department of Meteorology, Massachusetts Institute of Technology.

It is the non-axisymmetric flows that are most closely relevant to the dynamics of the atmosphere (Riehl & Fultz 1957). However, the axisymmetric flow, with which this paper is concerned, is extremely interesting in its own right as a fluid-dynamical problem and to a limited extent is analogous to the tropical trade-wind or Hadley circulation. More important, perhaps, is the fact that its study would seem to be an essential preliminary to the more difficult task of understanding the non-axisymmetric phenomena in detail.

The problem of describing theoretically even the axisymmetric flow is not straightforward; the simultaneous importance of buoyancy, Coriolis and viscous forces, coupled with advection and diffusion of heat, means that the mathematical problem is still *a priori* a formidable one. Early attempts at a theory appropriate to this general type of flow (see, for example, Davies 1953; Kuo 1954; Lorenz 1953) made use of assumptions that were unrealistic in one way or another, such as neglect of side boundary conditions. An approach involving assumptions of a rather different kind, concerning the specific form of the temperature field, for instance, has been used more recently by Hide (1967).

The first realistic theory of steady axisymmetric flow in the annulus was the boundary-layer theory given by Robinson (1959) for a rigidly bounded annulus of square cross-section and negligible curvature, and valid when the rate of rotation Ω is so large, relative to the imposed horizontal temperature contrast ΔT, that the heat transfer is conduction-dominated throughout the fluid. Under these circumstances the mathematical problem can be linearized (although it is still intricate) through the use of an expansion based on a small parameter involving $\Delta T/\Omega^2$. Robinson's original analysis is in error in certain respects, and has recently been corrected by Hunter (1967), who also gives new results concerning the modification of the flow fields by heat convection, and extends the analysis to the case of a free top surface.

As far as the writer is aware no comparable analytical theory, in which all the boundary conditions are satisfied and the approximation scheme is self-consistent and realistic, has previously been given for the contrasting situation in which $\Delta T/\Omega^2$ is relatively large and the heat transfer across the annulus is convection-dominated. The present work provides such a theory, based also on boundary-layer methods, for the rigidly bounded case. Although there is no linearizing expansion for the whole flow, a set of self-consistent and realistic approximations has been found that leads to a greatly simplified mathematical problem.

Within its region of validity, this theory forms a useful complement to the several recent numerical studies of the axisymmetric flow (Piacsek 1966; Quon 1967; Williams 1967). It is thought to provide a particularly apt example of how the process of finding a suitable approximate solution to a complicated fluid-dynamical problem can lead to a great deal of physical insight into the problem, particularly with regard to the way in which different regions in the flow, not necessarily adjacent to one another, interact to determine the flow as a whole. This kind of understanding would be difficult to achieve by simply examining the appropriate numerical solutions. On the other hand, the strength of the numerical approach lies in its minimal dependence on *a priori* assumptions, and the ideas upon which the present theory is based originally came from the

opportunity afforded the writer by Dr C. Quon to study and discuss some of the latter's recent numerical results.

A formal definition of the region of validity is postponed until §3 to allow the basic equations and parameters to be set up first in §2. The region of validity will be called the 'convective regime' to distinguish it from the conductive regime analysed by Robinson and Hunter.

Following §§2 and 3, we proceed to the details of the scale analysis in §4, and obtain a set of approximations valid in the limit of small boundary-layer thickness. In §§5 and 6 the individual boundary-layer solutions are obtained, and §7 completes the formulation of the 'primary problem', which is a closed problem that determines the boundary-layer flows together with integral properties of the interior such as the horizontally averaged zonal velocity. The primary problem can be thought of as expressing the main balances of the flow considered as a whole. The 'secondary problem' of subsequently determining the interior flow *details* is discussed qualitatively in §8. In §9 results are presented to illustrate the dependence of the primary problem upon its two determining parameters, and a preliminary comparison with numerical experiment is carried out. §10 summarizes the theory, and in §11 we give some concluding remarks and speculations.

Before going further, we draw attention to the fact that the approximation scheme upon which the theory is based has important features in common with that developed independently by Barcilon & Pedlosky (1967) in their linear theory of slow steady mechanically or thermally driven motions of a contained strongly stratified rotating fluid (the first of their three recent papers). Notable similarities are the thickness scale and essential physics of the side boundary layers, and the fact that viscosity and heat conduction are significant throughout the interior. The principal difference is that the present problem is fully non-linear, through both the horizontal and the vertical convection terms in the heat equation. The success of the present treatment stems largely from the fact that the greater part of the non-linearity is relegated to the secondary problem, and thus plays only a subsidiary role in the analysis and, by implication, in the physics of the flow.

2. Basic equations and parameters

We consider axisymmetric steady convection in an annulus of liquid rotating about its axis with angular velocity Ω as shown in figure 1, with a temperature difference $\Delta T'$ imposed between the perfectly conducting inner and outer cylindrical side walls. The horizontal boundaries are thermally insulating, and all four bounding surfaces are rigid.

The following assumptions defining a 'Boussinesq liquid' will be made at the outset: that density variations are negligible except in the buoyancy term, and that the coefficients ν, κ, α of viscosity, heat diffusivity and thermal expansion can be taken as constants (and that frictional heating is negligible). We shall also take the centrifugal acceleration to be negligible compared with gravity: $\Omega^2 R_2/g \ll 1$, where R_2 is the outer radius of the annulus. This is realistic for most

of the laboratory experiments, and moreover can in principle be satisfied as accurately as desired by scaling up the geometry. (Of course the latter device also improves the accuracy of the Boussinesq approximation, by reducing the values of ΔT required and hence reducing variations in ν.)

The problem thus defined will be taken as the starting-point. We note that the corresponding time-dependent equations are those used in the numerical studies referred to in the last section.

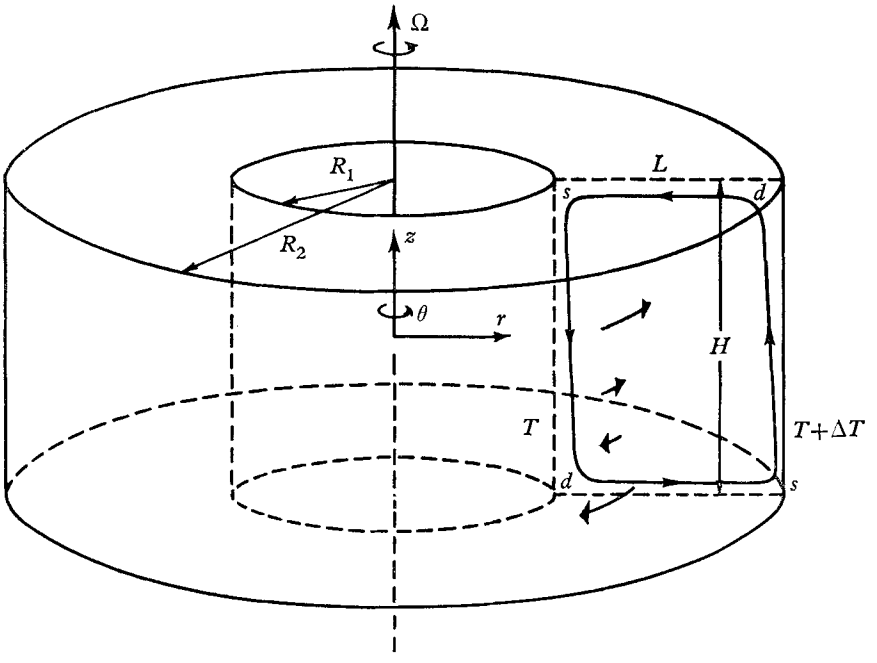

FIGURE 1. Definition sketch. The 'starting corners' (s) and 'departure corners' (d) are named from the point of view of the side boundary layers. (The terminology is that of Eckert & Carlson 1961.) A typical streamline of the meridional velocity field is sketched, and the zonal velocity field is indicated by the arrows.

The equations and boundary conditions will be written in the rotating frame of reference in terms of cylindrical polar co-ordinates (r, θ, z) as defined in figure 1, to which correspond the velocity components (u, v, w). The Boussinesq liquid is kinematically incompressible, so that a Stokes streamfunction Ψ may be used for the meridional velocities u, w. We adopt the convention

$$u = \frac{1}{r}\Psi_z, \quad w = -\frac{1}{r}\Psi_r,$$

so that the θ-component of vorticity is

$$\omega = +\frac{1}{r}\left(\frac{\partial^2}{\partial r^2} - \frac{1}{r}\frac{\partial}{\partial r} + \frac{\partial^2}{\partial z^2}\right)\Psi.$$

The equations of the problem may conveniently be taken as the θ-vorticity

equation together with the zonal momentum equation and the heat equation. These are

$$\frac{1}{r}\Psi_z\left(\omega_r-\frac{\omega}{r}\right)-\frac{1}{r}\Psi_r\omega_z=\nu\left(\nabla^2\omega-\frac{\omega}{r^2}\right)-g\alpha T_r+2\Omega v_z+\frac{2vv_z}{r}, \tag{2.1a}$$

$$\frac{1}{r}\Psi_z\left(v_r+\frac{v}{r}\right)-\frac{1}{r}\Psi_r v_z=\nu\left(\nabla^2 v-\frac{v}{r^2}\right)-\frac{2\Omega}{r}\Psi_z, \tag{2.1b}$$

$$\frac{1}{r}(\Psi_z T_r-\Psi_r T_z)=\kappa\nabla^2 T, \tag{2.1c}$$

where

$$\nabla^2\equiv\frac{\partial^2}{\partial r^2}+\frac{1}{r}\frac{\partial}{\partial r}+\frac{\partial^2}{\partial z^2},$$

and T is the temperature.

The boundary conditions are

$$\left.\begin{aligned} v=\Psi=\partial\Psi/\partial n=0 \text{ on all the boundaries,}\\ T=\text{a specified constant on each side wall,}\\ \partial T/\partial n=0 \text{ on each horizontal boundary,}\end{aligned}\right\} \tag{2.1d}$$

where $\partial/\partial n$ signifies a normal derivative. The imposed horizontal temperature difference is ΔT. For definiteness we shall consider the outer wall to be hotter than the inner one.

The problem defined above contains the seven physical parameters $g\alpha\Delta T$, $\Omega, \nu, \kappa, R_1, R_2$ and H (see figure 1). These involve dimensions of length and time only, and so the problem can be specified by five dimensionless parameters. A set such as the following is usually taken (we write L for R_2-R_1):

$\beta=g\alpha\Delta TH/4\Omega^2L^2$ (external thermal Rossby number),

$\epsilon=\nu/2\Omega L^2$ (Ekman number),

$\sigma=\nu/\kappa$ (Prandtl number),

$\left.\begin{aligned}\lambda=H/L\\ \rho=R_1/R_2\end{aligned}\right\}$ (aspect ratios).

3. Region of validity

Like the theory developed by Robinson and Hunter for the conductive regime, the present theory is based on boundary-layer analysis for small ϵ. The most important other parameter is $\beta\sigma$ (more precisely, $\beta\sigma\lambda^{-\frac{3}{2}}$; however λ, and ρ also, will be assumed to be of order unity as $\epsilon\to 0$). In the theory of the conductive regime $\beta\sigma$ is the small parameter of the linearizing expansion, and is assumed to be $o(\epsilon^{\frac{1}{2}})$, whereas the formal condition on $\beta\sigma$ appropriate to the present theory is $\beta\sigma\sim 1$, as $\epsilon\to 0$. As the scale analysis will show, this condition can be interpreted physically as saying that, while rotation is an important controlling influence in most parts of the flow, it is not strong enough to prevent a convectively dominated heat transfer across the annulus.

The Prandtl number σ will be assumed large; formally, $\sigma \gtrsim \epsilon^{-\frac{1}{2}}$ as $\epsilon \to 0$. It will be found that this is not too serious a restriction on the applicability of the theory. In analogous non-rotating laminar convective flows, the implied neglect of the convective acceleration terms is a very good approximation for $\sigma = 7$ (water) and even lower (Elder 1966; Gill 1966). The extent to which this may be true when rotation is present is not obvious, but it will be found still to be true in the side boundary layers, and the comparison with numerical experiment in §9 will indicate that, although for $\sigma = 7$ the approximation is not everywhere as good as in the side boundary layers, the errors are still not serious. This is fortunate, since the numerical values of $\beta\sigma$ for which the theory best describes the flow (these are found to be somewhat greater than 1) happen to correspond, when $\sigma = 7$, to the interesting transition region between the upper symmetric regime and the wave regime (Fowlis & Hide 1965; Barcilon 1964).

Finally, it will be found that the aspect ratio λ must be less than a certain critical value in the vicinity of 2. This somewhat unexpected restriction is due to the fact that if λ is too large the secondary problem for the interior flow details is not well posed. In §11 a conjecture is given as to the way in which the character of the flow changes when λ exceeds its critical value.

4. The scale analysis

We start by summarizing the main assumptions upon which it is convenient to base the scale analysis.

(i) $\beta\sigma \left(= \dfrac{g\alpha\Delta T H}{4\Omega^2 L^2} \dfrac{\nu}{\kappa} \right)$ is of order unity.

(ii) The aspect ratios $\lambda = H/L$ and $\rho = R_1/R_2$ are of order unity.

(iii) There are single thickness scales ℓ for the side and h for the top and bottom boundary layers.

(iv) The side boundary layers are *convective*: heat convection is as important as conduction, and the temperature scale is ΔT. (It follows that the side boundary-layer equations must be non-linear.)

(v) 'Outside' the boundary layers there is an interior flow characterized by the length scale L. (This scaling will turn out not to be uniformly valid in the neighbourhoods of the corners, although it will be valid at any fixed distance from them.)

(vi) The interior meridional velocities u, w are not substantially greater than the side boundary-layer vertical velocity (in fact it will turn out that they are far smaller), and the temperature scale in the interior is ΔT. The slopes of the interior isotherms are of order unity.

(vii) $\sigma (= \nu/\kappa) \gg 1$.

In terms of the side boundary-layer thickness ℓ, the basic approximation to be made is to neglect ℓ/L in comparison with unity. Symbols such as $\ll$, and various verbal expressions, are to be given the corresponding formal interpretations: for instance assumption (vii) means that $\sigma^{-1} = O(\ell/L)$ as $\ell/L \to 0$. The scale analysis is equivalent to taking the leading terms that arise in each flow region from a *formal* expansion procedure in powers of ℓ/L (or of $\epsilon^{\frac{1}{2}}$, as it turns out).

Before turning to details we summarize the key results.

(*a*) Coriolis forces, despite their importance elsewhere, may be neglected in the side boundary layers. The scale ℓ is given by $\ell^4 = \nu\kappa H/g\alpha\Delta T$.

(*b*) The top and bottom boundary layers may be taken as Ekman layers, and so $\hbar^2 = \nu/2\Omega$. Moreover, $\ell \sim \hbar(= \epsilon^{\frac{1}{2}}L)$.

(*c*) The meridional velocities in the interior are so small as to be negligible in the boundary-layer analysis; the mass flux of the meridional circulation, and with it the overall heat flux, is carried predominantly in the boundary layers. Viscosity and heat conduction, as well as horizontal and vertical heat convection, are important throughout the interior. The 'thermal wind equation' holds in the interior.

The side boundary layers

Clearly Ψ may be replaced by the local ordinary streamfunction ψ ($u = \psi_z$, $w = -\psi_r$) for each side wall boundary layer. With $\psi = \Psi/R_1$ for the inner wall or Ψ/R_2 for the outer wall, the equations (2.1) become, in the boundary-layer approximation,

$$\psi_z\psi_{rrr} - \psi_r\psi_{rrz} = \nu\psi_{rrrr} - g\alpha T_r + 2\left(\Omega + \frac{v}{r}\right)v_z, \tag{4.1a}$$

$$\psi_z v_r - \psi_r v_z = \nu v_{rr} - 2\Omega\psi_z, \tag{4.1b}$$

$$\psi_z T_r - \psi_r T_z = \kappa T_{rr}. \tag{4.1c}$$

Assumptions (iii) and (iv) applied to the heat equation (4.1*c*) lead directly to a single scale for ψ, namely

$$\psi(= r^{-1}\Psi) \sim \kappa H/\ell. \tag{4.2}$$

An immediate consequence is that the convective acceleration terms, which comprise the left-hand sides of the other two equations, are of order σ^{-1} times the viscous terms and may therefore be neglected, by assumption (vii).

In (4.1*a*) the viscous torque $\nu\psi_{rrrr}$ must be important in balancing the driving torque $-g\alpha T_r$. This balance may therefore be used to define ℓ, so that

$$\ell^4 = \frac{\nu\kappa H}{g\alpha\Delta T}. \tag{4.3}$$

We now show that the term $2(\Omega + v/r)v_z$ in (4.1*a*) is negligible. This is a major simplification, since (4.1*a*) and (4.1*c*) then form a closed system, being no longer coupled to (4.1*b*).

To obtain the required estimate for v we note that, in contrast to the balance in the boundary layers, the vorticity balance in the *interior* is dominated by the Coriolis and buoyancy torques. That is, equation (2.1*a*) may be replaced by

$$v_z = \frac{g\alpha}{2\Omega}T_r \quad \text{in the interior,} \tag{4.4}$$

the so-called 'thermal wind equation' familiar in geophysical fluid dynamics. (Using (4.2) and (4.3) one can verify that under assumptions (vi) and (vii) the convective acceleration and viscous terms in (2.1*a*) are respectively $O(\ell/L)$ and $O(\ell/L)^2$ times $g\alpha T_r$, in the interior. The term $2vv_z/r$ may be shown to be $O(\ell/L)$

times the Coriolis term $2\Omega v_z$, because of the relation $\beta \ll 1$ implied by assumptions (i) and (vii). This establishes the formal validity of (4.4); to forestall possible confusion it is just as well to note here that, even though in practical applications to the upper symmetric regime the numerical value of β approaches unity, neglect of $2vv_z/r$ against $2\Omega v_z$ usually remains a good approximation because the factor $\Delta T/L^2$ in β overestimates $r^{-1}T_r$.)

Returning now to the formal analysis of the boundary-layer equation (4.1*a*), we see that, if v_z is assumed not to be significantly greater in the boundary layer than in the interior, it follows very simply that $2\Omega v_z$, as well as $2vv_z/r$, is negligible against $g\alpha T_r$. For, as we move from the interior (where $2\Omega v_z = g\alpha T_r$) into the boundary layer, the scale for T_r goes up by an order of magnitude from $\Delta T/L$ to $\Delta T/\ell$ while the scale for v_z stays, at most, the same.

Equations (4.1*a*) and (4.1*c*) are now the same as their equivalents in the analogous non-rotating problem considered recently by Gill (1966). In dimensionless form, with the scales $\kappa H/\ell$ for ψ, ΔT for T, and H for z, they become

$$0 = \psi_{\xi\xi\xi\xi} - T_\xi, \tag{4.5a}$$

$$\psi_z T_\xi - \psi_\xi T_z = T_{\xi\xi}, \tag{4.5c}$$

where ξ is a stretched radial co-ordinate with scale ℓ.

It may be verified that equation (4.1*b*) reduces, formally, to $v_{\xi\xi} = 0$, which merely implies that to sufficient accuracy the zonal velocity has *no* side boundary layer of thickness ℓ. This might seem to suggest the possibility of a more complicated boundary-layer structure involving intermediate thickness scales such as $(L\ell)^{\frac{1}{2}}$, contrary to assumption (iii). But consideration of the interior flow vindicates assumption (iii), since it will be found that the interior zonal velocity can itself satisfy the no-slip condition. Indeed, it appears that it *must* do so, since it can be argued directly that the alternative possibility of an outer boundary layer is remote in the present problem. In brief this is because of the difficulty of reconciling a convectively dominated heat equation with the continuity equation and any reasonable configuration of the isotherms.

The viscous-conductive nature of the interior

Again invoking the formal relation $\beta \ll 1$ and the thermal-wind scale $v \sim g\alpha\Delta TH/2\Omega L$, we find that if the horizontal scale is L the convective acceleration terms in (2.1*b*) must be negligible against the Coriolis term (no matter what the Ψ and z scales are). To put it another way, a balance between the Coriolis and convective acceleration terms would signify that fluid particles were accelerating freely under the Coriolis force; particles so accelerating would over a radial distance L acquire zonal velocities that would be associated (using symmetry) with values of v_z too large to be compatible with the thermal-wind equation (4.4). Therefore the steady-state interior zonal momentum balance must be viscous-Coriolis, which immediately puts a stringent restriction on the horizontal velocity

$$r^{-1}\Psi_z \sim \frac{\nu}{2\Omega}\frac{v}{L^2}, \quad \sim \frac{\nu}{2\Omega}\frac{g\alpha\Delta TH}{2\Omega L^3} = \beta\sigma\frac{\kappa}{L}. \tag{4.6}$$

Because $\beta\sigma \sim 1$ this is an order of magnitude smaller than the horizontal velocity scale κ/ℓ characteristic of the side boundary layers. Note the important consequence that *entrainment from the interior is negligible in the analysis of the side boundary layers*, a direct result of the presence of rotation.

The relation $u = r^{-1}\Psi_z \sim \kappa/L$ applied to the heat equation (2.1*c*) shows at once that in the interior the horizontal convection term, and therefore both convection terms, are of the order of the conduction term. Further, from assumption (vi) $T_z \sim T_r$, and therefore

$$w \sim u, \sim \kappa/L, \quad \text{in the interior.} \tag{4.7}$$

We have thus arrived at the interesting picture of an interior flow *in which viscosity and heat conduction are important in the 'inviscid' limit* $\epsilon \to 0$. The interior equations are the full heat equation (2.1*c*), a zonal momentum equation (2.1*b*) in which only the right-hand side is retained, and the thermal wind equation (4.4). The associated mathematical problem will be discussed in §8, where it will be confirmed that *v can* satisfy the required side wall no-slip conditions, as is suggested by the 'viscous' nature of the zonal flow.

The top and bottom boundary layers

We know already that in (2.1*b*) only the viscous and Coriolis terms can be significant, by the remark made at the beginning of the last subsection. (The assumption that the v scale is no greater than in the interior has been made.) The side boundary-layer volume flux $\kappa H/\ell$ cannot flow through the interior, by (4.7), and must therefore be carried in the horizontal boundary layers. Therefore $r^{-1}\Psi \sim \kappa H/\ell$, and again using the assumption $v \lesssim g\alpha\Delta T H/2\Omega L$ we find from the viscous-Coriolis balance in (2.1*b*) that the scale $\hbar$ must satisfy

$$\hbar/\ell \lesssim \beta\sigma\lambda^{-1} \ (\sim 1) \tag{4.8}$$

and, consequently, that in (2.1*a*) the viscous term dominates every other term except $2\Omega v_z$.

Therefore the horizontal boundary-layer equations may be taken as

$$\nu r^{-1}\Psi_{zzzz} + 2\Omega v_z = 0, \tag{4.9a}$$

$$\nu v_{zz} - 2\Omega r^{-1}\Psi_z = 0, \tag{4.9b}$$

$$r^{-1}(\Psi_z T_r - \Psi_r T_z) = \kappa T_{zz}, \tag{4.9c}$$

and it follows that $\hbar$ may be defined by

$$\hbar = (\nu/2\Omega)^{\frac{1}{2}}, \quad = (\beta\sigma)^{\frac{1}{4}}\lambda^{-\frac{1}{2}}\ell \ (\sim \ell), \tag{4.10}$$

and that, in contrast to the situation near the side walls,

$$v \sim \hbar^{-1}r^{-1}\Psi, \quad \sim g\alpha\Delta T H/2\Omega L, \tag{4.11}$$

using $r^{-1}\Psi \sim \kappa H/\ell$ and $\beta\sigma \sim \lambda \sim 1$. It is obvious that no further terms can be dropped from (4.9*c*), since all the relevant scales are of the same order as the analogous scales in the side boundary layers.

The closed system (4.9*a*, *b*) describes the familiar Ekman layer, the heat equation (4.9*c*) posing a local forced-convection problem. We further note that,

like the side layers, *the Ekman layers may be taken as non-divergent*, because of the smallness of the interior vertical velocity $w \sim \kappa/L$ as compared to the formal scale $\kappa H/\ell L$ for w in the Ekman layer.

The analysis has depended crucially on assumption (i), $\beta\sigma \sim 1$. This relation expresses among other things the fact that, although for given ΔT the rotation Ω is strong enough to organize the flow near the horizontal boundaries into Ekman layers, it is not strong enough to prevent these layers from carrying a convectively generated volume flux from the side boundary layers. (If the rotation is significantly stronger, so that $\beta\sigma \ll 1$, a slight modification of the above chain of reasoning shows that there is *no* apparent way in which a volume flux of order $\kappa H/\ell$ per unit azimuthal distance can cross from one side wall to the other, in axisymmetric steady flow. It is for this reason, rather than because of changes in the local balances near the side walls, that when $\beta\sigma \ll 1$ the side boundary layers cease to be convective even though an appropriate Rayleigh number may be large. Conduction then becomes an important overall heat transfer mechanism throughout the fluid.)

5. The Ekman layers

Under the rigid-surface boundary conditions $v = \Psi = \partial\Psi/\partial n = 0$, and the non-divergence condition derived above, the meridional volume flux per radian being constant and equal to Ψ_I say, the solution of the system (4.9a, b) for the bottom boundary layer is

$$\Psi = \Psi_I\{1 - e^{-\zeta}(\sin\zeta + \cos\zeta)\}, \tag{5.1a}$$

$$v = -\frac{\sqrt{2}\,\Psi_I}{\hbar}\frac{1}{r}(1 - e^{-\zeta}\cos\zeta), \tag{5.1b}$$

so that

$$u = \frac{\sqrt{2}\,\Psi_I}{\hbar}\frac{1}{r}e^{-\zeta}\sin\zeta, \tag{5.2}$$

where

$$\zeta = (z + \tfrac{1}{2}H)/\sqrt{2}\,\hbar, \quad \hbar^2 = \nu/2\Omega.$$

The solution for the top boundary is obtained if ζ is re-defined as $(\frac{1}{2}H - z)/\sqrt{2}\,\hbar$ and the signs of u and v changed.

These solutions show that, once Ψ_I is specified, the zonal velocities at the top and bottom of the *interior* are

$$\left.\begin{matrix} v_{(t)} \\ v_{(b)} \end{matrix}\right\} = \pm\frac{\sqrt{2}\,\Psi_I}{\hbar}\frac{1}{r}. \tag{5.3}$$

Note that this implies that there is a discontinuity in the interior zonal velocity v at each corner, because of the no-slip condition on v at the sides. This is the reason for the non-uniformity of the scaling in the neighbourhoods of the corners. The presence of the discontinuity is however formally consistent, since orders of magnitude in equation (2.1b) are such that a fluid particle entering an Ekman layer from the adjoining departure-corner region can experience a zonal acceleration, under the Coriolis force, that is sufficient to give it the required zonal velocity of order $r^{-1}\Psi_I/\hbar$ by the time it has travelled a radial

distance of order ℓ. This depends on the assumption $\sigma \gg 1$ which implies, as required, that even in a corner region of length scale ℓ the convective acceleration terms of equation (2.1*b*) are not significantly greater than the Coriolis term; the viscous terms do not dominate the Coriolis term either, being comparable as in the Ekman layer itself.

6. The side boundary layers

Focusing attention on the inner or cold wall, so that $\xi = (r - R_1)/\ell$, we first integrate the dimensionless vorticity equation (4.5*a*) once to give the vertical momentum balance

$$T(\xi, z) - T_1(z) = \psi_{\xi\xi\xi} \,(= -w_{\xi\xi}). \tag{6.1}$$

To sufficient accuracy $w_{\xi\xi} \to 0$ as $\xi \to \infty$; therefore the function of integration T_1 is the interior temperature 'just outside' the boundary layer. It will be assumed that the vertical gradient $T_{1z} > 0$. Note that z runs between $\pm \frac{1}{2}$.

Elimination of T between (6.1) and (4.5*c*) gives a single equation for $\psi(\xi, z)$:

$$\psi_{\xi\xi\xi\xi\xi} - \psi_z \psi_{\xi\xi\xi\xi} + \psi_\xi (T_{1z} + \psi_{\xi\xi\xi z}) = 0. \tag{6.2a}$$

Adopting the convention that the dimensionless cold and hot wall temperatures are 0 and 1, we have $u = w = T = 0$ at the wall ($\xi = 0$), and $u, w, (T - T_1) \to 0$ as $\xi \to \infty$ (see §4). These boundary conditions may be written in terms of ψ as

$$\left.\begin{aligned} \psi &= 0 \\ \psi_\xi &= 0 \\ \psi_{\xi\xi\xi} &= -T_1(z) \end{aligned}\right\} \quad \text{at} \quad \xi = 0, \qquad \left.\begin{aligned} \psi &\to \text{const}\,(= \Psi_I) \\ \psi_\xi &\to 0 \\ \psi_{\xi\xi\xi} &\to 0 \end{aligned}\right\} \quad \text{as} \quad \xi \to \infty, \tag{6.2b}$$

where Ψ_I has now been made dimensionless, using the scale $R_1 \kappa H/\ell$.

As in the Ekman-layer problem, the boundary conditions cannot all be imposed independently. Just as solution of that problem yielded information about the interior zonal velocity (equation (5.3)), we might expect that the system (6.2), together with any conditions that need to be specified concerning the flow down into the boundary layer from the starting corner at $z = +\frac{1}{2}$, should imply something about the form of $T_1(z)$. In order to make this clearer we shall first consider a simplified problem, which contains the essential physics and, as will be found later, appears to approximate the full problem surprisingly well. The simplified problem is easily soluble, being the result of replacing (6.2*a*) by the linearized equation

$$\psi_{\xi\xi\xi\xi\xi} + T_{1z} \psi_\xi = 0. \tag{6.3}$$

(Note that the linearization is a valid approximation for large ξ.) The solution of (6.3) that satisfies all the boundary conditions (6.2*b*) except the one involving T_1 is

$$\psi(\xi, z) = \Psi_I \{1 - e^{-\eta}(\sin\eta + \cos\eta)\}, \tag{6.4a}$$

where

$$\eta(\xi, z) = (T_{1z})^{\frac{1}{4}} \xi / \sqrt{2}. \quad (T_{1z} > 0.)$$

Application of the remaining boundary condition results in a first-order ordinary differential equation for T_1, which upon integration yields the relation

$$T_1(z) = \frac{108\,\Psi_I^4}{(z_1 - z)^3}, \tag{6.4b}$$

where z_1 is a constant.

The solution (6.4) contains the two constants Ψ_I and z_1, which as yet are arbitrary. It is natural to regard these as being determined by conditions at the 'starting end' $z = \frac{1}{2}$, Ψ_I being the volume flux of the inflow, and z_1 then being determined by, say, the local temperature contrast $T_1(\frac{1}{2})$ across the end of the boundary layer. These two integral conditions represent all the information that can or need be specified at $z = \frac{1}{2}$. Diffusion down into the boundary layer of further starting-corner information, concerning the profile $\psi(\xi, \frac{1}{2})$ for instance, is negligible in the linearized problem (rather as in the Ekman-layer problem).

Now the *full* boundary-layer equation (6.2*a*) possesses an exact, self-similar solution which satisfies all the conditions (6.2*b*), and which can also satisfy both of the above-mentioned integral conditions on the inflow at $z = \frac{1}{2}$ (the values of Ψ_I and $T_1(\frac{1}{2})$). If further conditions were irrelevant to the full problem, as they are to the linearized problem, we could say immediately that this similarity solution is the required solution for the side boundary layer.

But the additional, non-linear terms in equation (6.2*a*) involve $\partial\psi/\partial z$, indicating that more does need to be specified at (say) $z = \frac{1}{2}$. Thus the similarity solution is only one of a family of possibly relevant solutions, *all* of which satisfy (6.2*b*) together with the two integral conditions at $z = \frac{1}{2}$, and we cannot determine which of these solutions is the correct one unless we have further information concerning the flow out of the starting corner. Fortunately, however, it happens that, even though the similarity solution may not be the strictly correct solution, it can be expected to be close to it numerically. Heuristic justification for this assertion will be given below; for the moment it will be *assumed* to be true. We shall then have in the similarity solution a simple analytical description of the side boundary-layer flow, and we shall also have avoided the difficult corner-flow problem, without, it is provisionally assumed, incurring serious error.

The similarity solution has the following form:

$$\left.\begin{aligned} &\psi = B_1 F(X), \\ \text{where} \quad &X = \frac{B_1 \xi}{z_1 - z} > 0 \quad (z_1 > \tfrac{1}{2}); \\ \text{also} \quad &T_1(z) = \frac{B_1^4}{(z_1 - z)^3}, \end{aligned}\right\} \tag{6.5}$$

where B_1 and z_1 are constants. $T_1(z)$ has exactly the same functional form as in the approximate solution (6.4); note that $B_1 = \Psi_I / F(\infty)$. The temperature in the boundary layer is

$$T_1 + \psi_{\xi\xi\xi} = \frac{B_1^4}{(z_1 - z)^3}(1 + F'''), \tag{6.6a}$$

and the dimensionless velocities (scales κ/ℓ, $\kappa H/\ell^2$) are

$$u = \psi_z = \frac{B_1^2 \xi}{(z_1 - z)^2} F', \tag{6.6b}$$

$$w = -\psi_\xi = -\frac{B_1^2}{z_1 - z} F'. \tag{6.6c}$$

F is the universal function defined by

$$F^{\mathrm{v}} + 3F' + 3F'F'''' = 0; \tag{6.7a}$$

$$\left.\begin{aligned} F = F' &= 0 \\ F'''' &= -1 \end{aligned}\right\} \quad \text{at} \quad X = 0; \qquad F', F'''' \to 0 \quad \text{as} \quad X \to \infty. \tag{6.7b}$$

The system (6.7) is easy to solve by iteration. Posing

$$F' = aF_1' + a^2 F_2' + a^3 F_3' + \ldots, \tag{6.8a}$$

where a is yet to be determined, we may satisfy (6.7a) and all the relevant boundary conditions of (6.7b) except the inhomogeneous one, at each order in a, by

$$\left.\begin{aligned} F_1' &= e^{-\eta} \sin \eta, \\ F_2' &= -\frac{\sqrt{3}}{30} e^{-2\eta} \sin 2\eta, \\ F_3' &= \frac{1}{1600}\{e^{-3\eta}(5 \sin 3\eta + 3 \sin \eta + 9 \cos \eta) - 9\, e^{-\eta} \cos \eta\}, \\ &\ldots\ldots\ldots\ldots\ldots\ldots\ldots\ldots\ldots\ldots, \end{aligned}\right\} \tag{6.8b}$$

where now

$$\eta(\xi, z) = (\tfrac{3}{4})^{\frac{1}{4}} X = 0{\cdot}93X, \quad = \frac{0{\cdot}93 B_1 \xi}{z_1 - z}. \tag{6.9}$$

These three terms give more than enough accuracy; imposing the remaining boundary condition $F'''' = -1$ at $X = 0$ gives $a = 1{\cdot}18/\sqrt{3}$. Also

$$F(\infty) = \int_0^\infty F' dX, \quad = 0{\cdot}36 \quad (0{\cdot}35_9),$$

so that

$$\Psi_I = 0{\cdot}36 B_1. \tag{6.10}$$

We shall require later the value of

$$\int_0^\infty F'(1 + F'''') dX, \quad = 0{\cdot}26. \tag{6.11}$$

Two terms are sufficient for evaluating the integrals.

The rapidity of convergence of the series (6.8) is remarkable, and shows that under the conditions of the similarity solution the influence of the non-linear terms in (6.2a) is weak. It can be verified directly that the exact solution is very well approximated by (6.4), the solution to the linearized problem. The effect of the second and higher terms of (6.8) upon the shapes of the velocity profiles is almost imperceptible, and is only slightly more noticeable in the temperature profile. If a were set equal to $1/\sqrt{3}$ instead of $1{\cdot}18/\sqrt{3}$, and the constant 0·36 in

(6.10) replaced by $108^{-\frac{1}{4}}$, $= 0{\cdot}31$, and the higher terms of (6.8) ignored, the similarity solution would become identical with (6.4). The smallness of the non-linear effects is presumably connected with the strong constraint of zero entrainment.

Some justification can now be given *a posteriori* for the assumption made earlier, that the similarity solution is close to the strictly correct solution corresponding to the actual inflow from the starting corner. We recall that it is the non-linear terms in (6.2*a*) that involve the z-derivatives which allow diffusion along the boundary layer of starting-corner information more detailed than that represented by the values of Ψ_I and $T_1(\frac{1}{2})$. Inasmuch as the influence of the non-linear terms is small, the effect of the additional information will be weak, even though not formally negligible as it is in the linearized problem. Thus, even if the additional information is specified incorrectly at $z = \frac{1}{2}$, so as to lead for instance to the similarity solution instead of to the strictly correct solution, the difference

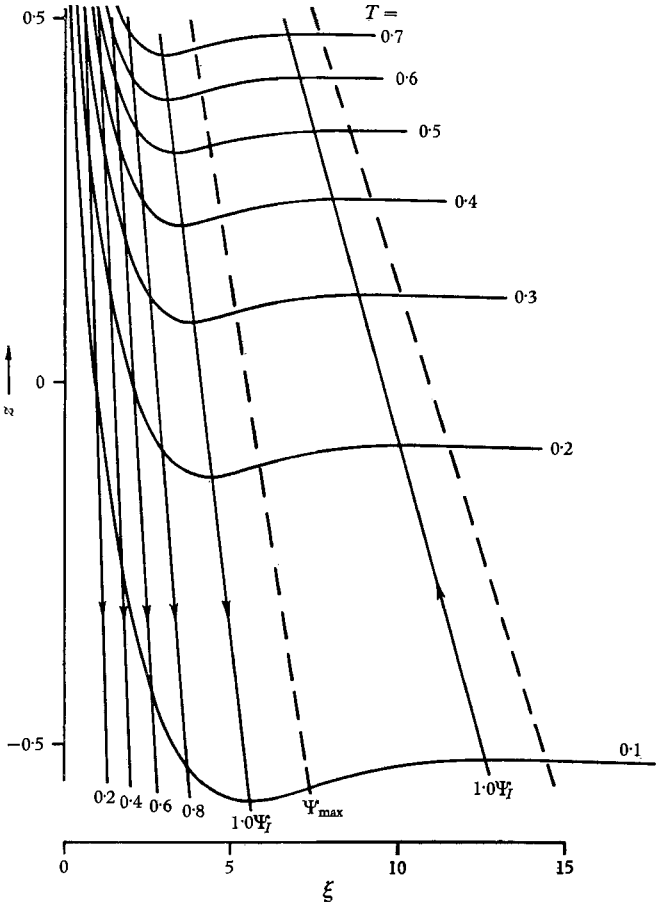

FIGURE 2. Isotherms and streamlines for the cold wall boundary-layer similarity solution (6.5) with $z_1 = 1{\cdot}58$, $B_1^4 = 0{\cdot}93$. The dashed lines indicate the first region of reverse flow; $\Psi_{max} \simeq (1+e^{-\pi})\Psi_I$. (This flow reversal and the superficially similar phenomenon found in the conductive-regime side boundary layers occur for quite different dynamical reasons.)

between the two solutions can be expected to be numerically small except in the vicinity of the starting corner.

These remarks provide heuristic justification only, since it is possible, of course, that the inflow conditions could be so different from those corresponding to the similarity solution that the non-linear terms become more important than an estimate based on the similarity solution would suggest. Further investigation, probably involving numerical solution of (6.2) and perhaps of the corner flow problem, would be required to settle this question and to provide a quantitative error estimate. In the meantime it can be noted that the present ideas seem to be supported by the comparison with numerical experiment in §9.

The similarity-solution isotherm and streamline patterns are illustrated in figure 2. It is worth remarking that the overshoot of the temperature past its interior value, indicated by the shape of the isotherms, is a characteristic feature of any side-wall boundary layer for which the principal dynamical balance is between buoyancy and viscous forces and for which $w \to 0$ as $\xi \to \infty$. For $w(\xi)$ must then have (at least) one point of inflexion, and the momentum balance (6.1) shows that $T(\xi, z) - T_1(z)$ must therefore change sign. In other words, the downward velocity of the heavy fluid near the cold wall cannot be brought smoothly back toward zero as we move toward the interior, unless there is an *upward* buoyancy force on the fluid a little further out from the wall.

When the Prandtl number σ is finite, a similarity solution is still possible, and may be used to estimate the effect on the side boundary layers of the neglected convective acceleration terms. For $\sigma = 7$ this solution is found to be almost indistinguishable from the solution (6.5), differences being typically less than 1 %. This suggests that, except near the corners, the side boundary layers will be among the places where finite-σ effects are least noticeable.

7. Formulation of the complete primary problem

Equality of the boundary-layer volume fluxes has already been utilized implicitly; another relation connecting the four boundary layers with each other, this time directly through their relationship with the interior, is the thermal wind equation (4.4) integrated over the interior:

$$\int_{R_1}^{R_2} (v_{(t)} - v_{(b)})\, dr = \frac{g\alpha}{2\Omega} \int_{-\frac{1}{2}H}^{\frac{1}{2}H} (T_2 - T_1)\, dz,$$

where $v_{(t)}(r)$, $v_{(b)}(r)$ are the top and bottom interior zonal velocities, given in terms of Ψ_I by (5.3), and $T_1(z)$, $T_2(z)$ are the interior side temperatures near the cold and hot side walls. The latter are given in dimensionless form by (6.5), (6.10), and their analogues for the hot wall involving, say, the constants B_2 and $z_2 (< -\frac{1}{2})$. That is,

$$T_1(z) = \frac{B_1^4}{(z_1 - z)^3}, \quad T_2(z) = 1 - \frac{B_2^4}{(z - z_2)^3}, \tag{7.1}$$

where $0{\cdot}36 B_1 = \Psi_I$, $0{\cdot}36 B_2 = \rho \Psi_I$. The aspect ratio ρ appears asymmetrically because of the way in which Ψ_I was made dimensionless in §6, scale $R_1 \kappa H / \ell$.

Upon substitution for $v_{(t)}$, $v_{(b)}$, T_1 and T_2 in the integrated thermal wind equation, making all variables dimensionless, we obtain

$$\Psi_I, = 0{\cdot}36B_1 = 0{\cdot}36B_2\,\rho^{-1},$$

$$= \mu\tau\left[1 - \tfrac{1}{2}B_2{}^4\left\{\frac{1}{(-\frac{1}{2}-z_2)^2} - \frac{1}{(\frac{1}{2}-z_2)^2}\right\} - \tfrac{1}{2}B_1{}^4\left\{\frac{1}{(z_1-\frac{1}{2})^2} - \frac{1}{(z_1+\frac{1}{2})^2}\right\}\right], \tag{7.2}$$

where

$$\tau = \frac{1}{2\sqrt{2}}\frac{\hbar^3 H}{\ell^3 L}, \quad = (\tfrac{1}{4}\beta\sigma)^{\frac{3}{4}}\lambda^{-\frac{1}{2}}, \tag{7.3}$$

and

$$\mu = \frac{1-\rho}{\rho\ln(1/\rho)}. \tag{7.4}$$

Now (7.2) gives two relations connecting B_1, B_2, z_1 and z_2. We still need to make some statement about the side boundary-layer starting-end temperature contrasts $T_1(\frac{1}{2})$ and $1-T_2(-\frac{1}{2})$, which are clearly connected via the corresponding Ekman layers with temperatures in the opposite departure corners. This will lead to the two further relations required. Although a strict derivation of these relations would involve solution of the Ekman-layer forced convection problem, it will turn out that a detailed analysis can be avoided at the cost of introducing small errors only, in the following way.

Consider the boundary-layer heat equation (4.9*c*). The velocity field is given by (5.1), and consequently the heat equation reduces to $uT_r = \kappa T_{zz}$; note that ru is a function of z only. The boundaries are insulators, and to sufficient accuracy there is no conductive heat exchange with the interior. We may therefore derive the following integral relations for, say, the bottom Ekman layer:

$$\int_0^\infty ruT\,dz = \text{constant}, \quad = \overline{T}\int_0^\infty ru\,dz \quad \text{say},$$

and

$$\frac{\partial}{\partial r}\int_0^\infty ru(T-\overline{T})^2 dz = -2\kappa r\int_0^\infty T_z^2 dz, \; <0,$$

where $z\to\infty$ implies the inner or boundary-layer limit. Thus with respect to ru considered as a weighting function, the cross-boundary-layer temperature distribution has constant mean $\overline{T}$ and decreasing variance as we move 'downstream'. In using these concepts we are treating ru as if it were one-signed; thus we suppose that the regions of small negative values of ru outside the main part of the boundary layer are not of qualitative importance in the forced convection problem.

Now figure 3*a* shows the temperature profile near the lower end of the cold wall layer. If the flow round the departure corner is smooth, the temperature profile at the beginning of the Ekman layer must be qualitatively as shown in figure 3*b* (convection dominates conduction in the corner), so that the fluid is coldest next to the lower boundary. If we now move along the Ekman layer toward the hot wall, the temperature mean stays constant and the variance decreases, as was shown, and it is presumed that the only reasonable way in which this can happen is for the fluid to become warmer next to the boundary

and colder in the outer part of the layer. That is, the horizontal temperature gradient $\partial T_{(b)}/\partial r$ just above the Ekman layer is *negative*. On the other hand, this gradient can be expected to be weak ($L\,\partial T_{(b)}/\partial r$ numerically much smaller than ΔT), since the cold wall boundary-layer fluid has given up much of its heat by the time it reaches the departure corner, so that the profiles in figures 3*a* and *b* involve only a rather small overall temperature difference. Furthermore, only a certain fraction of this will be felt by the outer parts of the Ekman layer.

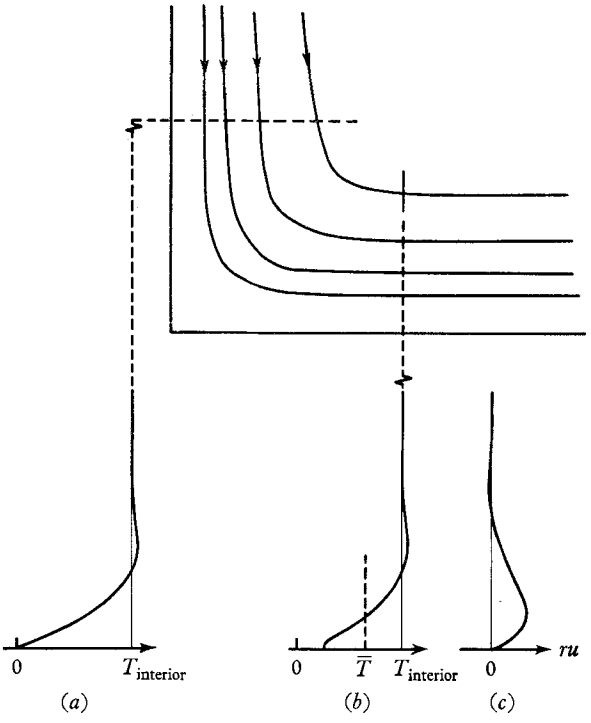

FIGURE 3. Temperature and velocity profiles near the cold wall departure corner (see text).

This suggests that it would be a good approximation merely to set $\partial T_{(b)}/\partial r = 0$, i.e. to assert that the bottom of the interior is isothermal. (This approximation may well be even better in practice than in the limit $\epsilon \to 0$. In the numerical experiment referred to in §9, finite-ϵ effects render $\partial T_{(b)}/\partial r$ slightly *positive*; see figure 7*b* below.) The same arguments apply to the top Ekman layer.

We postulate, then, that *the top and bottom of the interior are isothermal.* We then have $T_1(\frac{1}{2}) = T_2(\frac{1}{2})$ $(= T_{(t)}$ say) and $T_2(-\frac{1}{2}) = T_1(-\frac{1}{2})$ $(= T_{(b)})$. Thus, from (7.1),

$$\frac{B_1^4}{(z_1-\frac{1}{2})^3} + \frac{B_2^4}{(\frac{1}{2}-z_2)^3} = 1, \tag{7.5}$$

$$\frac{B_1^4}{(z_1+\frac{1}{2})^3} + \frac{B_2^4}{(-\frac{1}{2}-z_2)^3} = 1. \tag{7.6}$$

Together with (7.2) these are sufficient to determine all the unknowns in terms of the two external parameters τ and ρ, and with them the boundary-layer solu-

tions, and the horizontally averaged interior zonal velocity $\bar{v}$ which in dimensionless form, scale $\kappa H/\ell\hbar$, is

$$\bar{v}(z) = -\frac{\sqrt{2}}{\mu}\Psi_I + 2\sqrt{2}\,\tau\left[\tfrac{1}{2}+z+\tfrac{1}{2}B_2^4\left\{\frac{1}{(z-z_2)^2}-\frac{1}{(-\frac{1}{2}-z_2)^2}\right\}\right.$$
$$\left.-\tfrac{1}{2}B_1^4\left\{\frac{1}{(z_1-z)^2}-\frac{1}{(z_1+\frac{1}{2})^2}\right\}\right]. \qquad (7.7)$$

It will be useful also to derive an expression for the total Nusselt number or dimensionless heat transfer. This should not be calculated by integrating the local Nusselt number of the similarity solution, since an important contribution from the thermally active starting corner would then be ignored, but on the other hand we may calculate Nu from the difference between the convective heat fluxes at the departure-corner ends of the two side boundary layers. (The heat flux entering each Ekman layer is the same as that which leaves it, to sufficient accuracy.) At the bottom of the cold wall boundary layer, remembering the convention $T = 0$ on the cold wall, we may write the outgoing convective temperature flux per radian as $R_1\kappa H\Delta T/\ell$ times the dimensionless quantity

$$\left[\int_0^\infty \psi_\xi(T_1+\psi_{\xi\xi\xi})\,d\xi\right]_{z=-\frac{1}{2}},$$
$$= \frac{B_1^5}{(z_1+\frac{1}{2})^3}\int_0^\infty F'(1+F''')\,dX = \frac{0{\cdot}72\Psi_I B_1^4}{(z_1+\frac{1}{2})^3}, \qquad (7.8)$$

using (6.5), etc. If there were no convection, the purely conductive temperature flux per radian would be $R_1\kappa H\Delta T\times\mu/L$. Subtracting (7.8) from its analogue for the top of the hot wall boundary layer, and dividing by $\mu\ell/L$, we obtain the Nusselt number as

$$Nu = \frac{L\Psi_I}{\ell\mu}\left[1-0{\cdot}72\left\{\frac{B_2^4}{(\frac{1}{2}-z_2)^3}+\frac{B_1^4}{(z_1+\frac{1}{2})^3}\right\}\right]. \qquad (7.9)$$

Notice that $Nu \propto \Delta T^{\frac{1}{4}}$, if Ω is made $\propto\Delta T^{\frac{1}{2}}$ so that τ is fixed. The dependence of Nu on τ, and thus for instance on ΔT for fixed Ω, is clearly more complicated (cf. Bowden & Eden 1965, p. 187*a*; Williams 1967, p. 172*b*).

8. The interior flow

Before going further we shall briefly discuss, without solving, the secondary problem of determining the details of the interior flow. Numerical solution is presumably feasible, but would be unlikely to lead to new insight.

The interior equations were found in §4 to be

$$g\alpha T_r - 2\Omega v_z = 0, \qquad (4.4), (8.1a)$$

$$\nu r\left(\nabla^2 v - \frac{v}{r^2}\right) - 2\Omega\Psi_z = 0, \qquad (8.1b)$$

$$\kappa r\nabla^2 T + T_z\Psi_r - T_r\Psi_z = 0, \qquad (2.1c), (8.1c)$$

where ∇^2 is the cylindrical Laplacian as in (2.1). The boundary conditions are determined by the primary problem. They are, in dimensional form,

$$\left.\begin{aligned} v = 0\,(\therefore T_r = 0), \quad T = T_i(z) \quad \text{at} \quad r = R_i\ (i = 1, 2), \\ v = \begin{cases} v_{(t)}(r) \\ v_{(b)}(r) \end{cases} \quad T = \begin{cases} T_{(t)} \\ T_{(b)} \end{cases} \quad \text{at} \quad z = \begin{cases} \frac{1}{2}H, \\ -\frac{1}{2}H, \end{cases} \end{aligned}\right\} \tag{8.1d}$$

recalling (5.3), (7.1), the remarks preceding (7.5), and those following (4.5c). A point of interest is that there are no boundary conditions on Ψ. This expresses the fact that fluid can enter or leave the boundary layers at the very small velocity characteristic of the interior, without in the first approximation affecting the main balances of the flow.

It can be argued (McIntyre 1967, p. 58) that the gross features of the interior Ψ, v and T fields are somewhat as sketched in figure 4. The corner singularity is the reason for the non-uniform validity of the scaling near the corners. The formally valid approximate condition of no entrainment into the side boundary layers becomes, for any fixed value of ϵ, increasingly less well satisfied as the

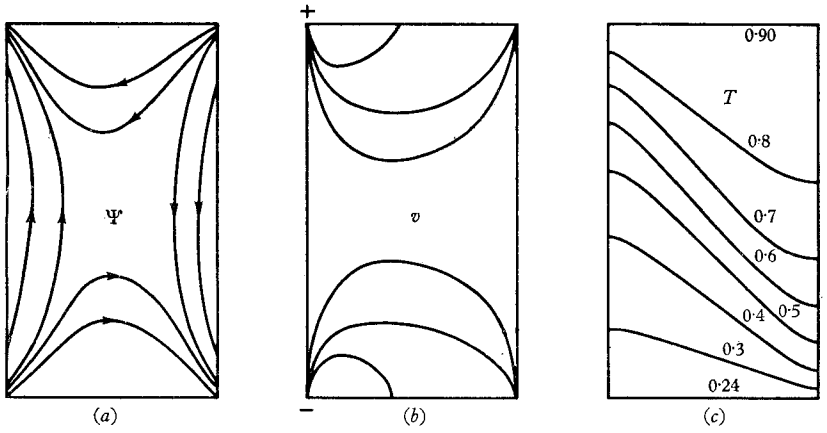

FIGURE 4. Contour diagrams of plausible interior Ψ, v and T fields. The inner or cold wall $r = R_1$ is on the left. The 'boundary' temperatures in (c) correspond to the case $\rho = 0{\cdot}62$, $\tau = 1{\cdot}86$ (see § 9), but otherwise the diagrams are schematic. The zonal velocity v takes its extreme values at the upper and lower inner corners, and is discontinuous at all four corners. The meridional velocity probably goes infinite in each corner. Note that a consequence of the conditions $T = T_{(t)}, T_{(b)}$ at $z = \pm\frac{1}{2}H$ is that $v_z = 0$ at $z = \pm\frac{1}{2}H$.

corner is approached. In cases of practical interest, this is thought to be a greater source of error in the side boundary-layer solutions than the neglect of conditions within the starting corner discussed in § 6.

It is not immediately obvious whether or not (8.1) can be a well-posed boundary-value problem. However, if the equations are rewritten as a set of four first-order equations in the dependent variables $\partial T/\partial r$, $\partial T/\partial z$, $\partial(rv)/\partial r$, Ψ, there are two independent conditions on each boundary and it can be shown (Courant & Hilbert 1962, p. 171) that the system is elliptic at a given point provided

$$\lambda < \tau^{-2}S^{-3}G^{-\frac{3}{2}}; \tag{8.2}$$

$G = HT_z/\Delta T$ is the dimensionless vertical temperature gradient and

$S = |LT_r/HT_z|$ is a scaled slope of the isotherm through the given point. This ellipticity criterion depends on the unknown solution of (8.1) because of the non-linearity of the system.

It is only the presence of the horizontal convection term $-T_r\Psi_z$ in (8.1*c*) that prevents the system from being elliptic when λ is large. This suggests that, for tall annuli, convection might dominate conduction in at least part of the interior, the streamlines there lying along the isotherms. As in the non-rotating analogue (Gill 1966), information would then be carried through the interior from one side boundary layer to the other and would have to be accounted for in the boundary-layer analysis itself, precluding a breakdown into primary and secondary problems.

In the next section we shall make estimates of the right-hand side of (8.2), based on the assumption of plausible smoothly varying temperature fields such as that suggested in figure 4*c*. We shall thus ignore, as has already been tacitly done in the discussion that led to (7.5) and (7.6), the detailed structure that must actually be present near the corners because of the weak corner singularities. (In fact (8.2) *is* probably violated near the corners, for any λ, but this local ill-posedness is thought not to be of great importance in practice. Although as $\epsilon \to 0$ one might expect eventually to see, in theory, some change in the character of the interior flow very near each corner, it is believed that the values of $\epsilon^{\frac{1}{2}}$ and σ^{-1} involved would be too small to be of practical interest. But if the interior problem (8.1) were being solved numerically, some *ad hoc* smoothing of the boundary condition on v might be necessary.)

It seems relevant to note that (8.2) can be shown also to represent a criterion for dynamical stability to infinitesimal axisymmetric disturbances. It is not the same as the classical inviscid criterion of Solberg (see Ooyama 1966); the instability associated with violation of (8.2) represents a viscosity-caused destabilization, for large Prandtl number, of a flow which is *stable* by the classical criterion.

9. Numerical results

Dependence on τ and ρ

The primary problem has been reduced to solving the algebraic equations (7.2), (7.5) and (7.6), given the values of τ and ρ. The dependence of the interior side temperature distributions (7.1) on τ and ρ is illustrated in figure 5, in which the left- and right-hand diagrams give the positions of the interior isotherms at $r = R_1$ and R_2 respectively. In figure 4*c* above, the temperature distributions at the edges of the interior correspond to the case marked by the dotted lines ($\tau = 1{\cdot}86$, $\rho = 0{\cdot}62$) in figure 5.

The main feature of the τ-dependence, illustrated by the top half of figure 5, is that the average slope of each interior isotherm increases as τ becomes smaller, i.e. as Ω is increased or ΔT decreased. We can look at this effect in the following way. An increase in Ω tends to reduce the volume flux per radian (Ψ_I) in the Ekman layers, both because the Ekman layers become thinner and because, in

the interior, v_z decreases for given T_r. A corresponding diminution in the volume flux carried by the side boundary layers, whose thickness scale ℓ remains constant if ΔT is fixed, gives fluid particles in them more time in which to gain or lose heat over a given vertical distance. Thus vertical temperature gradients

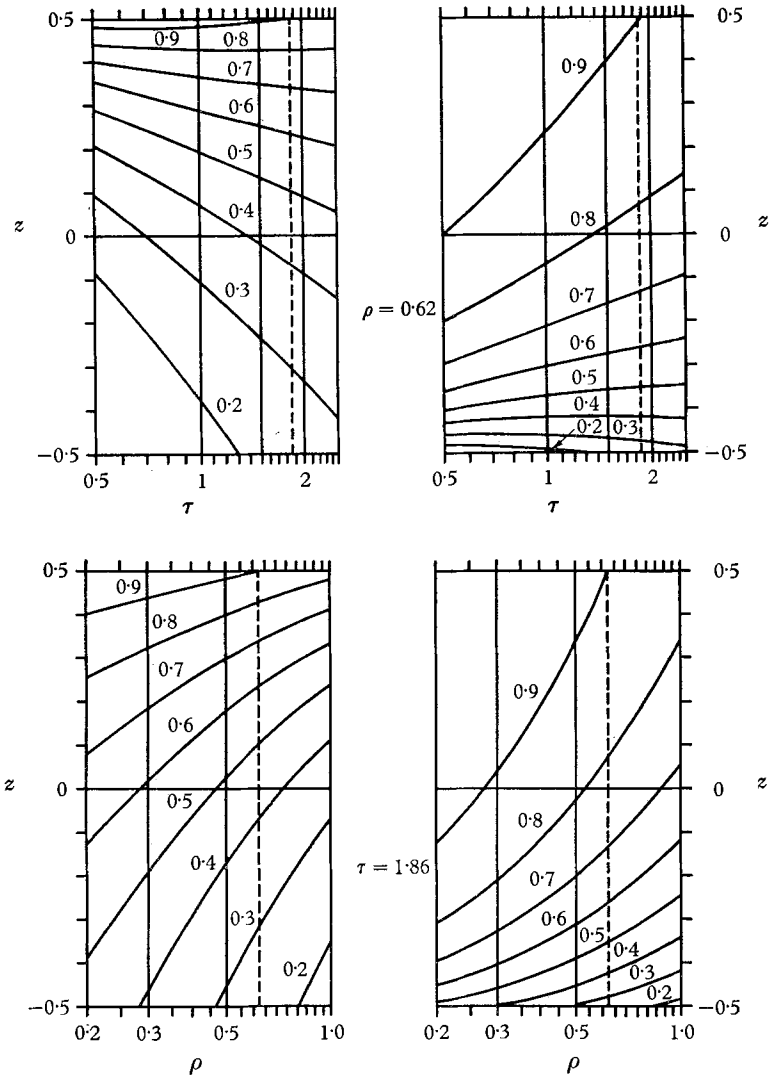

FIGURE 5. Isotherm diagrams illustrating the dependence of the interior side temperature distributions on τ (top) and on ρ (bottom). The left- and right-hand diagrams give respectively the inner ($r = R_1$) and outer ($r = R_2$) side temperature distributions.

tend to become more concentrated near the starting corners, and the average slope of each interior isotherm must increase until a new balance is attained.

When curvature is negligible ($\rho = 1$; see the lower pair of diagrams in figure 5), the problem is 'centro-symmetrical' (Gill 1966, p. 518). The most obvious consequence of finite curvature ($\rho < 1$) is that the inner boundary layer has to

carry a greater volume flux per unit azimuthal distance than the outer one. Thus, for instance, the fluid in it does not come as near to acquiring the wall temperature as occurs in the outer boundary layer, so that any given isotherm will be found lower and lower down in the interior as the curvature increases ($\rho\downarrow$). (The opposite would occur if the heating were reversed.) Further, it can be seen why the concentration of the vertical temperature gradient near the starting corner is more marked for the outer wall.

Figure 6 illustrates the dependence on τ and ρ of Ψ_I, $\ell Nu/L$ ($\propto \Delta T^{-\frac{1}{4}} Nu$), z_1 and z_2. (In connexion with the above, note that $|z_2| \leqslant |z_1|$.)

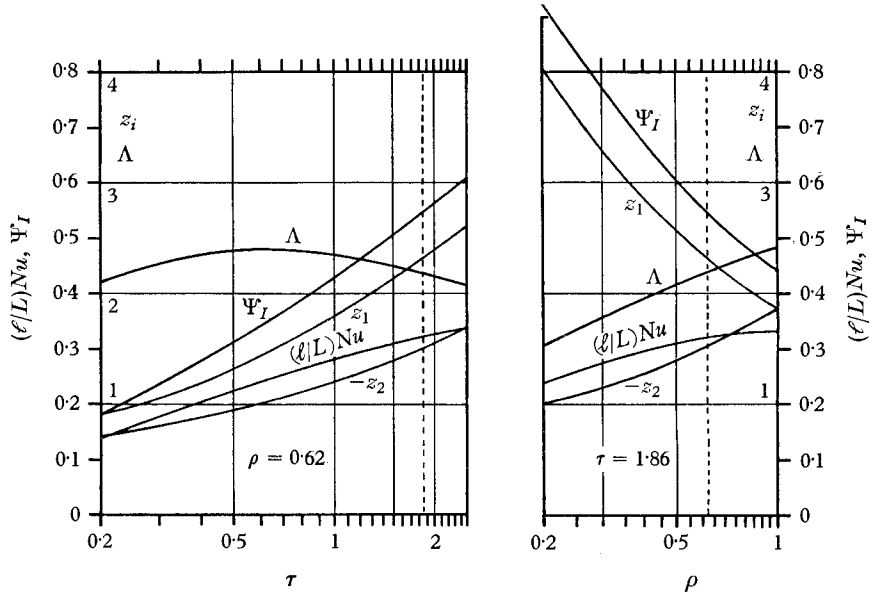

FIGURE 6. Illustrating the dependence of Ψ_I, $(\ell/L)Nu$, z_1, $-z_2$, and Λ, on τ (left-hand diagram) and on ρ (right-hand diagram).

In order to obtain some idea of the maximum permissible value of λ that would allow the interior problem to be well-posed (but see in this connexion the remarks at the end of §8), we also plot in figure 6 a rough estimate Λ of the minimum value of the right-hand side of the ellipticity criterion (8.2). For definiteness and for simplicity Λ is defined as the minimum value, over the interior, of $\tau^{-2}S^{-3}G^{-\frac{3}{2}}$ as it would be if the interior isotherms were straight lines. Consideration of plausible isotherm fields such as the one shown in figure 4*c* suggests that this is an overestimate, but on the other hand it will appear below that finite-ϵ effects work in the opposite direction. In practice the graphs of Λ are probably as good a guide as any to the maximum permissible value of λ. They are still only a rough guide, and could appropriately be summarized by simply saying that, as a provisional working rule, the theory can be expected to break down in practice if λ is greater than a value in the neighbourhood of 2. (Therefore geometries as tall as those used by Bowden & Eden (1965) in their rigid-lid experiments ($\lambda \simeq 3, 5$) seem definitely outside the scope of the theory.)

Finite-ϵ effects and comparison with numerical experiment

Of the rigid-lid numerical results available at present the best choice for comparison, having the smallest value of ϵ as well as a value of $\beta\sigma$ appropriate to the theoretical convective regime, is the case A 2 computed by Williams (1967), for which $\epsilon^{\frac{1}{2}} = 0{\cdot}0334$, $\beta\sigma = 5{\cdot}15$, $\sigma = 7{\cdot}19$, $\beta = 0{\cdot}716$, $\lambda = 1{\cdot}97$ and $\rho = 0{\cdot}578$ ($\tau = 0{\cdot}86$, $\mu = 1{\cdot}33$).† A 40×60 mesh was used. Williams's results for Ψ, T and v are reproduced in figure 7.

Although $\epsilon^{\frac{1}{2}} = 0{\cdot}0334$ is more than sufficiently small for the flow to have a well-developed boundary-layer character, it will be found that certain $O(\epsilon^{\frac{1}{2}})$ errors in the theory are still not very small numerically and, moreover, tend to reinforce each other. On the other hand, some of these errors can be corrected for in a simple and intuitively reasonable way, as will be done in the comparison that follows.

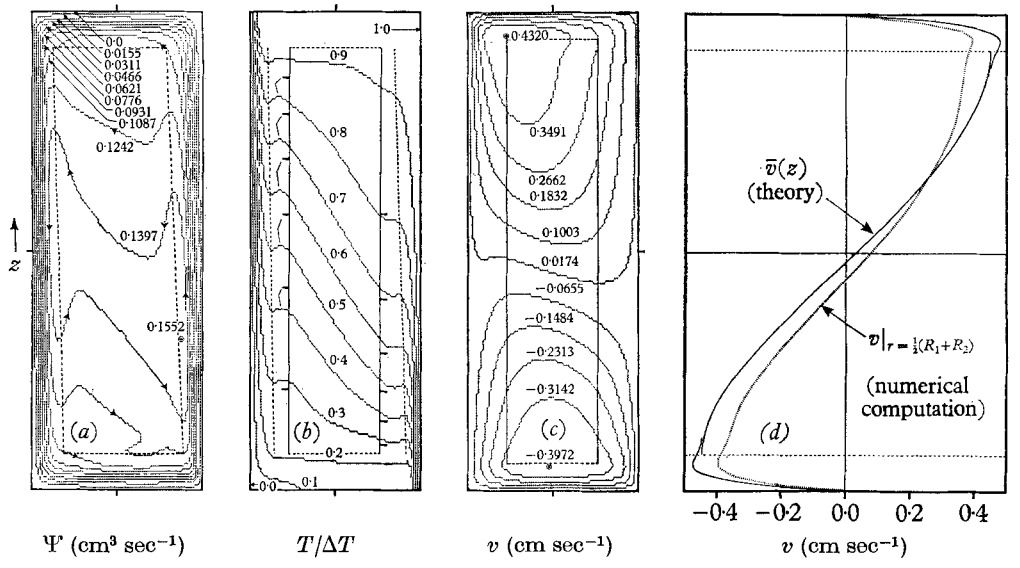

FIGURE 7. Results of the numerical computation A 2 of Williams (1967), compared with theory; see text below. In the equal-interval contour diagrams (*a*), (*b*) and (*c*) the inner or cold wall ($r = R_1$) is on the left. The vertical scale is exaggerated, the true aspect ratio $\lambda = H/L$ being 1·97. In (*d*), the theoretical curves (thin unbroken lines) give the interior and boundary-layer zonal velocities horizontally averaged over the inner width L_I (shown in (*c*)), whereas the other curve is the numerical result for v at $r = \frac{1}{2}(R_1 + R_2)$ (Williams, unpublished). The theoretical curve would be slightly *further* away from a numerical $\bar{v}(z)$ curve; the theoretical maximum and minimum values of $\bar{v}$ at top and bottom are 1·2$_7$ times the corresponding numerical values. The units are c.g.s., appropriate to $H = 5$ cm ($R_1 = 3{\cdot}48$ cm, $R_2 = 6{\cdot}02$ cm) and $\kappa = 1{\cdot}42 \times 10^{-3}$ cm^2 sec^{-1} ($\nu = 1{\cdot}008 \times 10^{-2}$ cm^2 sec^{-1})

First, the effective size of the interior is diminished by the finite thickness of the boundary layers. In the derivation of (7.2), the thermal wind equation $2\Omega v_z = g\alpha T_r$ was taken to hold over the full annulus cross-section of width L, as is

† *Note added in proof.* The value $\sigma = 7{\cdot}19$, and consequently the values of $\beta\sigma$, and τ, are slightly in error; σ should be 7·10. This makes no significant difference to the results below.

valid in the limit $\epsilon \to 0$. But, for the case under consideration, the width L_I of the region over which the thermal wind equation holds is only about $\frac{1}{2}L$. This can easily be shown from an estimate based on the theory, or can here be seen at once from figure 8 (Williams 1967), which shows the vorticity balance at $z = 0$ in the numerical experiment. It is clear that we can remove a major source of inaccuracy by re-deriving (7.2) using the thermal wind equation integrated over an interior region of width L_I only. The choice of L_I should represent a compromise such that the thermal wind equation is reasonably well satisfied over the inner region, the latter being, nevertheless, sufficiently wide for the temperature distributions at its sides to be still closely connected with the boundary layers. (The sides $r = R_{1I}, R_{2I}$ of the inner region that we shall define below are indicated in figures 7*b* and *c*, and in figure 8.)

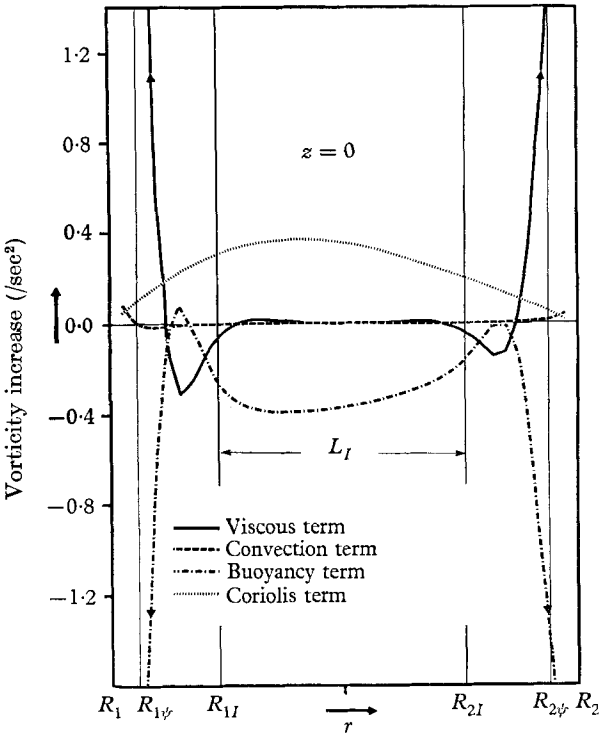

FIGURE 8. Significant terms in the vorticity equation (2.1*a*) at mid-height ($z = 0$), after Williams (1967).

We should also consider the inner region to have a reduced height H_I, such that the thermal wind equation does not become too inaccurate near the top and bottom ends, which, nevertheless, extend far enough into the outer parts of the Ekman layers for the top and bottom isothermal conditions (7.5) and (7.6) to hold. It will be useful then to define

$$\ell_I = (\nu\kappa H_I/g\alpha\Delta T)^{\frac{1}{4}}, \quad = \ell(H_I/H)^{\frac{1}{4}},$$

since the scale for z will be taken as H_I in order that the top and bottom boun-

daries of the inner region, where the isothermal conditions are to be imposed, remain at $z = \pm\frac{1}{2}$.

Purely for the sake of definiteness, we shall place these boundaries at the first theoretical Ekman-layer zeros of u (shown in figures 7*a*, *b*, *d* by dotted lines), a choice which seems as appropriate as any. The value of H_I is not as critical as the value of L_I, because H_I will appear only to the power $\frac{1}{4}$ and, in the present case, because $H > L$. The corresponding value of H_I is

$$H_I = H - 2 \times \pi \sqrt{2}\, \hbar. \tag{9.1}$$

Note that the complete inner region that we shall use is that shown in figure 7*b*. With regard to choosing the sides $r = R_{1I}$, R_{2I} and thence $L_I = R_{2I} - R_{1I}$, it can be verified from theoretical estimates that a rule adequate in most circumstances (with $\epsilon \doteq 10^{-3}$ or smaller) is simply to take points $\frac{3}{4}$ of the way from the first theoretical viscous-torque zero to the second in each side boundary layer, at $z = 0$. That is (ignoring higher terms in (6.8)!)

$$L_I = R_{2I} - R_{1I}, \tag{9.2}$$

where

$$\begin{Bmatrix} R_{1I} - R_1 \\ R_2 - R_{2I} \end{Bmatrix} = \frac{\frac{3}{2}\pi \ell_I}{0{\cdot}93} \begin{Bmatrix} |z_1|/B_1 \\ |z_2|/B_2 \end{Bmatrix} \doteq 5\ell_I \begin{Bmatrix} |z_1|/B_1 \\ |z_2|/B_2 \end{Bmatrix}.$$

In the relations $\psi = \Psi/R_1, \psi = \Psi/R_2$ for the side boundary-layer ordinary streamfunctions, the relevant modified values of R_i are not the same as R_{iI}, but should correspond to representative positions within the boundary layers where most of the mass transport and heat convection is taking place. Distances $1\frac{1}{2}$ times further from the walls than the principal maxima of w at height $z = 0$ are taken as being reasonable. The distances of the maxima are almost exactly $\frac{1}{4}\pi\ell_I|z_i|/0{\cdot}93B_i$, so that for calculating the ψ's the radii are taken as

$$\left.\begin{aligned} R_{1\psi} &= R_1 + 1{\cdot}3\ell_I|z_1|/B_1, \\ R_{2\psi} &= R_2 - 1{\cdot}3\ell_I|z_2|/B_2. \end{aligned}\right\} \tag{9.3}$$

Thus, also $B_2 = \rho_\psi B_1$, where $\rho_\psi = R_{1\psi}/R_{2\psi}$.

It is simplest to take the scale for Ψ as $R_{1\psi}\kappa H_I/\ell_I$. The scale for z is H_I. Then it can be shown that the modified primary problem, resulting from the use of (9.3) and from integration of the thermal wind equation over the inner region only, is still expressed by (7.2), (7.5) and (7.6) provided ρ, τ and μ are replaced by ρ_ψ,

$$\left.\begin{aligned} \tau_I &= \frac{1}{2\sqrt{2}} \frac{\hbar^3 H_I}{\ell_I^3 L_I} \\ \text{and} \qquad \mu_I &= \frac{L_I}{R_{1\psi} \ln (R_{2I}/R_{1I})}. \end{aligned}\right\} \tag{9.4}$$

A further correction that can legitimately be made for the purposes of the comparison, but which would be harder to estimate in the absence of the numerical results, since it depends among other things on the details of $v(r, z)$, is some allowance for the fact that the side boundary layers carry a greater volume flux per radian than do the Ekman layers. If ϕ denotes a representative value of the ratio of side flux to Ekman flux, it is clear that applying this correction is equivalent simply to multiplying the right-hand side of (7.2) by the factor ϕ; Ψ_I is

then to be interpreted as the side flux. To estimate ϕ from figure 7*a*, we must decide upon some value representative of the side volume fluxes, which vary considerably with height. We appeal to the fact that, as may easily be verified directly, the outer side boundary-layer temperature distribution can be fitted closely to that of the similarity solution if the flux of the similarity solution is in the neighbourhood of the actual *maximum* flux.† We thus have a rationale for basing the correction factor ϕ on the maximum side flux,

$$\doteq (1+e^{-\pi})^{-1} \times 0{\cdot}155 \text{ cm}^3 \text{ sec}^{-1}.$$

(This is not the same as imposing the desired answers on the analysis; the actual flux values that will emerge from solution of the full corrected primary problem remain to be seen.) Inspection of figure 7*a* now suggests $\phi \doteq 1{\cdot}3$, and a crude general rule for estimating ϕ is then

$$\phi = 1 + 0{\cdot}3 \frac{\epsilon^{\frac{1}{2}}\lambda}{(\epsilon^{\frac{1}{2}}\lambda)_{A2}} \doteq 1 + 4{\cdot}5\,\epsilon^{\frac{1}{2}}\lambda. \tag{9.5}$$

(This assumes λ not small, and is obtained by supposing that in the interior $\nu(\nabla^2 v - v/r^2)$ is approximately proportional to $\nu v_{(l)}/L^2$ at some radius r so that, by (8.1*b*) and (5.3), $ru \propto \hbar\Psi_I/L^2$, whence $\phi - 1 \propto ruH/\Psi_I \propto \epsilon^{\frac{1}{2}}\lambda$.)

Summarizing, the above corrections can be made *by simply replacing* $\mu\tau$ *in* (7.2) *by* $\mu_I\tau_I\phi$ *and using* $B_2 = \rho_\psi B_1$. Among the effects not allowed for are the influence of the mass exchange with the interior on the forms of the side boundary-layer solutions themselves (we have already indicated that for the outer boundary layer in the present case this is not serious provided that we estimate ϕ as above), and possible departures from the Ekman flux relation (5.3).

For the zonal velocity, τ, μ and Ψ_I in (7.7) should be replaced by τ_I, μ_I and Ψ_I/ϕ; the scale is $\kappa H_I/\ell_I\hbar$. In the expression (7.9) for Nu, L/ℓ should be replaced by $LR_{1\psi}H_I/R_1H\ell_I$ (μ being unaltered); all that we can say about Ψ_I, unfortunately, is that it should be replaced not by Ψ_I/ϕ but by some value between Ψ_I/ϕ and Ψ_I, since some heat will be convected (and conducted) across the interior.

Results

We have $H = 1{\cdot}97L$, $\hbar = 0{\cdot}0334L$, $H_I = 1{\cdot}67L$, $\ell_I = 0{\cdot}0299L$, $R_1 = 1{\cdot}37L$, $R_2 = 2{\cdot}37L$. The rules (9.1)–(9.5) together with (7.5), (7.6) and the modified version of (7.2) lead to $\{R_{1\psi}, R_{1I}, R_{2I}, R_{2\psi}\} = \{1{\cdot}43, 1{\cdot}60, 2{\cdot}13, 2{\cdot}31\}L$, $L_I = 0{\cdot}53L$, $\rho_\psi = 0{\cdot}62$, $\mu_I\tau_I\phi = 1{\cdot}30 \times 1{\cdot}55 \times 1{\cdot}3 = 2{\cdot}6$ ($\mu\tau$ is merely $1{\cdot}33 \times 0{\cdot}86 = 1{\cdot}15$!), $z_1 = 2{\cdot}41$, $z_2 = -1{\cdot}58$, $B_1^4 = 6{\cdot}3$, $B_2^4 = 0{\cdot}93$, $\Psi_I = 0{\cdot}57$.

When $H = 5$ cm and $\kappa = 1{\cdot}42 \times 10^{-3}$ cm^2 sec^{-1} as in $A\,2$, the theoretical side-boundary-layer maximum value of the Stokes streamfunction is very nearly $(1+e^{-\pi})\Psi_I \times R_{1\psi}\kappa H_I/\ell_I$ cm^3 sec^{-1}, $= 0{\cdot}17_1$ cm^3 sec^{-1}, 10% higher than the maximum value $0{\cdot}15_5$ cm^3 sec^{-1} in the middle portions of the side boundary layers in figure 7*a*. The dotted lines in figure 7*a* mark the theoretical first zeros of w for the side and u for the horizontal boundary layers. In figure 7*b* the dotted lines at the sides mark, instead, the theoretical first zeros of $\partial T/\partial r$.

† The appropriateness of something like the maximum, rather than an average, side flux is supported by a physical argument similar to that given in Gill (1966, p. 524). (Positive entrainment tends to reduce dT_1/dz or dT_2/dz, and vice versa.)

Also shown in figure 7*b* are the theoretical positions of the isotherms at the sides of the interior, obtained from (7.1). (The theoretical temperatures at $z = \pm\frac{1}{2}$, i.e. on the horizontal dotted lines, are 0·90, 0·25.) The discrepancy at the inner side represents a departure from the *form* of the similarity solution: there is no B_1, z_1 such that the side temperature distribution is closely represented by $B_1^4(z_1 - z)^{-3}$. This appears to be due to entrainment and ejection (see footnote above) rather than to starting-corner effects (§6); there is no indication that the discrepancy is associated particularly with the starting end of the boundary layer. Moreover, the outer side temperature distribution is well described by the theoretical expression, $1 - 0{\cdot}93(z + 1{\cdot}58)^{-3}$, especially near the starting end, where there is less entrainment than for the inner wall. The theoretical outer-wall similarity solution is the hot-wall equivalent of the solution shown in figure 2.

In the zonal velocity diagram 7*c*, the dotted lines indicate the theoretical first maximum of $|v|$ in each Ekman layer. The thin curves in figure 7*d* are the theoretical interior and boundary-layer zonal velocities horizontally averaged over L_I; also shown is the numerical result for v at $r = \frac{1}{2}(R_1 + R_2)$ (Williams, unpublished). The curves are of course not quite comparable, and the agreement is slightly *less* good than a casual glance might suggest. The dimensionless theoretical values of $\bar{v}_{(i)}$ and $\bar{v}_{(b)}$ are $\pm 0{\cdot}48$, scale $\kappa H_I/\ell_I \hbar$, corresponding to $\pm 0{\cdot}45$ cm sec^{-1} when $H = 5$ cm and $\kappa = 1{\cdot}42 \times 10^{-3}$ cm^2 sec^{-1}. These are about $1{\cdot}2_7$ times the corresponding quantities in $A\,2$ roughly estimated from figures 7*c*, *d*, which is consistent with the discrepancy in the interior isotherm slopes. (It is of interest to note further thermal-wind correlations between figures 7*b* and *d*.) The difference, evident in figure 7*c*, between the r-dependences of the top and bottom boundary layers indicates a departure from the Ekman solutions due to convective accelerations, a finite-σ effect. The influence of the $2v v_z/r$ term seems to be noticeable also.

Williams's value of Nu is 8·3. The two theoretical extremes, involving Ψ_I/ϕ and Ψ_I, are respectively 7·3, 9·4.

The estimate Λ should be replaced by Λ_I, involving τ_I; $\Lambda_I \doteq 3{\cdot}7$, to be compared with $\lambda_I = H_I/L_I \doteq 3{\cdot}1$. The interior equations are certainly elliptic for the temperature field of the *numerical experiment*, although the tendency of the streamlines to lie along the isotherms could be interpreted as saying that the equations are on the point of ceasing to be elliptic and would not be so if λ were much larger.

10. Summary of the main features of the theory

The boundary-layer approximation for small ϵ has been used to analyse the convective regime $\beta\sigma \sim 1$ (cf. the conductive regime $\beta\sigma = o(\epsilon^{\frac{1}{2}})$) of axisymmetric steady convection in a differentially heated rotating annulus, under the additional assumption of large $\sigma\,(\gtrsim \epsilon^{-\frac{1}{2}})$.

Since $\beta\sigma \gtrsim 1$ the side boundary layers are convective, and drive the whole flow. They are described by the same approximate equations as in convection in a (non-rotating) rectangular slot at high Rayleigh number, and have the same

single thickness scale $(\nu\kappa H/g\alpha\Delta T)^{\frac{1}{4}}$. The isotherms have the inflected shape characteristic of a stably stratified interior and a viscous-buoyancy dynamical balance. These side boundary layers are completely unlike those of the conductive regime, which are forced by the rest of the flow and in which the rotational coupling between Ψ and v is important. (The latter boundary layers are more nearly analogous to the present *interior* flow.)

Solution of the side boundary-layer equations, under the rotationally imposed condition of no entrainment from the interior, leads to information about the interior vertical temperature distribution 'just outside' each boundary layer. These distributions are of the form given by (7.1) and are determinate if the (constant) boundary-layer meridional volume flux per radian Ψ_I is specified, together with another condition such as the temperature contrast across the starting end of the boundary layer. The analysis ignores further details of the inflow from the starting corner, which is not strictly permissible, but it is argued that the resulting error is numerically small.

The Ekman layers also are non-divergent, because of the combined effects of rotation and stratification in the interior, and must also carry the constant volume flux Ψ_I. The interior zonal velocity just outside them is therefore $\pm 2(\Omega/\nu)^{\frac{1}{2}}\Psi_I/r$ for the top and bottom respectively, away from the corner regions. This means that Ψ_I is connected with the interior temperature field in another way, through the thermal wind equation $2\Omega v_z = g\alpha T_r$. Upon integration over the whole of the interior, this equation relates vertical differences of zonal velocity, and thus Ψ_I, to horizontal temperature differences. Therefore Ψ_I is related in a second way to the interior temperature distributions just outside the side boundary layers, without reference to the details of the interior flow.

These side temperature distributions, the top and bottom zonal velocities, and therefore, through the thermal wind equation, the horizontally averaged zonal velocity at each height z, are the interior quantities involved in the primary problem.

Finally, the temperature contrast across the starting end of each side boundary layer is related via the corresponding Ekman layer to temperatures in the opposite departure corner. These two relations suffice to close the primary problem. It is argued that to a very good approximation the two relations can be expressed simply by the statement that the top and bottom of the interior region are *isothermal*. This is a simplification which, together with the neglect of starting-corner flow details in the side boundary-layer analysis, and the neglect of the interior corner-singularity effect referred to at the end of §8, prevents the theory from being 'strictly valid' as $\epsilon \to 0$. However, in practice the $O(1)$ errors so introduced seem a good deal smaller numerically than certain of the (formally negligible) $O(\epsilon^{\frac{1}{2}})$ errors, such as those due to side boundary-layer entrainment.

The integral properties of the interior fields that are determined by solving the primary problem now become boundary conditions on the secondary problem of determining the interior flow details. Small meridional velocities, which are negligible in relation to the boundary layers, play an essential role in the interior. They are of order ϵv, $\sim \kappa/L$, and are necessary, first, to provide a Coriolis force which can maintain the zonal velocity field against viscous retardation, and

second, to provide just enough heat convection to maintain the interior temperature field against conductive relaxation, and in such a way that the thermal wind equation is satisfied.

The primary problem depends on the order-unity parameters $\tau, = (\frac{1}{4}\beta\sigma)^{\frac{3}{4}}\lambda^{-\frac{1}{2}}$, and ρ. The secondary problem depends on λ also, and breaks down if λ is greater than a critical value, roughly 2.

The numerical accuracy of the theory at finite ϵ can be greatly improved by making $O(\epsilon^{\frac{1}{2}})$ corrections based, for instance, on the simple rules (9.1)–(9.5), that make some allowance for obvious sources of error such as the reduction of the effective size of the interior due to finite boundary-layer thickness.

11. Concluding remarks

The regions in parameter space accessible to the 'corrected' theory only just overlap those that have been reached so far by the numerical method: the comparison in §9 shows discrepancies that are most sharply illustrated by the horizontally averaged interior zonal velocity, whose theoretical value is about 1·27 times that of the numerical experiment. These remaining discrepancies appear to be largely attributable to errors such as the departure (due to entrainment from the interior) of the inner side boundary-layer temperature distribution from that of the theoretical similarity solution.

Comparison with a laboratory experiment at smaller $\epsilon\,(< 10^{-3})$ would be desirable, with λ between 1 and 2, say. Unfortunately, it is not appropriate to take σ very much larger than 7 in a laboratory experiment (although $\sigma = 15$ or 20 would be worth consideration), since the wave regime would then be encountered for any reasonable value of $\beta\sigma$ and so of τ. If $\sigma = 7$ is chosen, the theory should predict the flow best for a geometry in which curvature effects are minimized (ρ as near 1 as practicable), and for as small a value of τ as can be attained without transition to the wave regime occurring. These conditions will minimize finite-σ effects in those parts of the flow where they tend to be most perceptible in the primary problem, namely near the corners and in the Ekman layers. The value of ϵ should be considerably less than 1×10^{-3} if possible. Finite-ϵ corrections such as those given by the rules (9.1)–(9.5) should still be made. (Note that (9.5) is a particularly crude estimate, and may possibly warrant refinement.)

Among the theoretical predictions suitable for testing in the laboratory are the vertical temperature distributions, given by (7.1), just outside each side boundary layer (about $5\ell_I|z_i|/B_i$ from each side wall—see (9.2)), and the temperatures at distances of about $\pi\sqrt{2}\,\epsilon^{\frac{1}{2}}L$ from the horizontal boundaries. The latter temperatures should be found to be approximately independent of r, away from the corners (§7). The total Nusselt number could be measured and compared with (7.9); but note that it is not obvious how to interpret Ψ_I in (7.9) for finite ϵ. Good measurements of the zonal velocity peak $(1 + e^{-3\pi/4}/\sqrt{2})v_{(0)}(r)$ at distance $\frac{3}{4}\pi\sqrt{2}\,\epsilon^{\frac{1}{2}}L$ below the lid might be feasible, perhaps using a photochemical dye method (Goldish *et al.* 1965).

The breakdown of the theory for λ greater than about 2 (§§8, 9) raises questions as to the nature of the flow in a tall annulus such as Bowden & Eden's (1965).

If the formal assumption $\lambda \sim \epsilon^{-\frac{1}{2}}$ is made, a scaling can be obtained under which the heat equation is convection-dominated throughout the interior. The simplifying feature of a breakdown into primary and secondary problems is then lost (§8). When λ is large but fixed as $\epsilon \to 0$ the situation is presumably even more complicated. What probably happens is that *part* of the interior becomes convection-dominated while the remainder still involves heat conduction, in a way similar to that indicated for the case of a free upper surface by the numerical results of Piacsek (1966) and Williams (1967). It would be interesting to carry out a rigid-lid numerical experiment for small ϵ with $\lambda = 3$, say, in order to see whether a tendency for the interior to split into subregions does indeed manifest itself.

This paper is based on part of the writer's doctoral research carried out at the University of Cambridge under F. P. Bretherton, who has had a deep influence upon this and other work, and whose interest and encouragement is gratefully acknowledged. The writer would also like to thank in particular C. Quon for the discussions which originally led to the present ideas. A further important influence has been the work of A. E. Gill and J. W. Elder on non-rotating convection. Helpful comments were contributed by a referee for the paper and by V. Barcilon and P. B. Rhines; G. P. Williams kindly supplied suitable copies of the diagrams presenting his results, published and unpublished, for the case A 2.

This work was supported by a Commonwealth Scholarship awarded by the Commonwealth Scholarship Commission in the United Kingdom. Some rewriting was done at the Woods Hole Oceanographic Institution and at the Meteorology Department, M.I.T., with support from National Science Foundation Grants GZ-419 and GA-402X respectively.

REFERENCES

Barcilon, V. 1964 Role of the Ekman layers in the stability of the symmetric regime obtained in a rotating annulus. *J. Atmos. Sci.* **21**, 291.

Barcilon, V. & Pedlosky, J. 1967 Linear theory of rotating stratified fluid motions. *J. Fluid Mech.* **29**, 1.

Bowden, M. & Eden, H. F. 1965 Thermal convection in a rotating fluid annulus: temperature, heat flow and flow field observations in the upper symmetric regime. *J. Atmos. Sci.* **22**, 185.

Courant, R. & Hilbert, D. 1962 *Methods of Mathematical Physics*, vol. II. New York: Interscience.

Davies, T. V. 1953 The forced flow of a rotating viscous liquid which is heated from below. *Phil. Trans.* A **246**, 81.

Eckert, E. R. G. & Carlson, W. O. 1961 Natural convection in an air layer enclosed between two vertical plates with different temperatures. *Int. J. Heat Mass Trans.* **2**, 106.

Elder, J. W. 1966 Numerical experiments with free convection in a vertical slot. *J. Fluid Mech.* **24**, 823.

Fowlis, W. W. & Hide, R. 1965 Thermal convection in a rotating annulus of liquid: effect of viscosity on the transition between axisymmetric and non-axisymmetric flow regimes. *J. Atmos. Sci.* **22**, 541.

Fultz, D., Long, R. R., Owens, G. V., Bohan, W., Kaylor, R. & Weil, J. 1959 Studies of thermal convection in a rotating cylinder with some implications for large-scale atmospheric motions. *Meteorol. Monographs*, **4**, no. 21.

GILL, A. E. 1966 The boundary-layer regime for convection in a rectangular cavity. *J. Fluid Mech.* **26**, 515.

GOLDISH, L. H., KOUTSKY, J. A. & ADLER, R. J. 1965 Tracer introduction by flash photolysis. *Chem. Eng. Sci.* **20**, 1011.

HIDE, R. 1958 An experimental study of thermal convection in a rotating liquid. *Phil. Trans.* A **250**, 441.

HIDE, R. 1967 Theory of axisymmetric thermal convection in a rotating fluid annulus. *Phys. Fluids*, **10**, 56.

HUNTER, C. 1967 The axisymmetric flow in a rotating annulus due to a horizontally applied temperature gradient. *J. Fluid Mech.* **27**, 753.

KUO, H.-L. 1954 Symmetrical disturbances in a thin layer of fluid subject to a horizontal temperature gradient and rotation. *J. Meteorol.* **11**, 399. (Also in Saltzman, B. 1962 *Theory of Thermal Convection*. New York: Dover.)

LAMBERT, R. B. & SNYDER, H. A. 1966 Experiments on the effect of horizontal shear and change of aspect ratio on convective flow in a rotating annulus. *J. Geophys. Res.* **71**, 5225.

LORENZ, E. N. 1953 A proposed explanation for the existence of two regimes of flow in a rotating symmetrically-heated cylindrical vessel. *Proc. First Symp. on the Use of Models in Geophys. Fluid Dyn.*, p. 73 (ed. R. R. Long).

MCINTYRE, M. E. 1967 Convection and baroclinic instability in rotating fluids. Ph.D. thesis, University of Cambridge.

OOYAMA, K. 1966 On the stability of the baroclinic circular vortex: a sufficient criterion for instability. *J. Atmos. Sci.* **23**, 43.

PIACSEK, S. 1966 Thermal convection in a rotating annulus of liquid: numerical studies of the axisymmetric regime of flow. Ph.D. thesis, Mass. Inst. of Technology.

QUON, C. 1967 Numerical study of thermal convection in a rotating fluid system. Ph.D. thesis, University of Cambridge.

RIEHL, H. & FULTZ, D. 1957 Jet stream and long waves in a steady rotating-dishpan experiment: structure of the circulation. *Quart. J. Roy. Meteorol. Soc.* **83**, 215.

ROBINSON, A. R. 1959 The symmetric state of a rotating fluid differentially heated in the horizontal. *J. Fluid Mech.* **6**, 599.

WILLIAMS, G. P. 1967 Thermal convection in a rotating fluid annulus, Parts I and II. *J. Atmos. Sci.* **24**, 144, 162.